RF magnetron sputtering of arsenic-doped p-type zinc oxide

Micah Nathaniel Shelley

A thesis submitted to the faculty of

Brigham Young University

In partial fulfillment of the requirements for the degree of

Bachelor of Science

Dr. John Colton PhD, Advisor

Department of Physics and Astronomy

Brigham Young University

April 27, 2019

Copyright © 2019 Micah Nathaniel Shelley

All Rights Reserved

ABSTRACT

RF magnetron sputtering of arsenic-doped p-type zinc oxide

Micah Nathaniel Shelley

Department of Physics and Astronomy

Bachelor of Science

Zinc oxide is a semiconductor with a wide band gap (3.37 eV), allowing for applications in optics and optoelectronics. Historically, stable p-type material has been difficult to create. We report deposition of stable p-type ZnO thin films by rf magnetron sputtering. Arsenic acts as the p-type dopant, and is provided through a base layer of Zn_3As_2 evaporated onto the substrate. Annealing the samples improves crystal structure. P-type material is confirmed, and material properties are quantified by Seebeck effect, Hall effect, photoluminescence, and x-ray diffraction measurements. We identify the effects of substrate temperature, sputter time, rf power, and plasma gas ratio on the electrical and optical properties of the ZnO:As. Future work to improve the quality of the films produced is discussed.

Keywords: zinc oxide; arsenic; zinc arsenide; p-type; magnetron sputtering; thin films;

semiconductor

Acknowledgments

I would like to thank John Colton, David Allred, and Gary Renlund for mentoring me in this work. Additional thanks to Ryan Peterson, Colter Stewart, James Erikson, Spencer King, Nathan Schwartz, and Emma McClure, who have worked on various parts of this project with me.

Table of Contents

List of Figures

List of Tables

1 Introduction

1.1 Motivation

Zinc oxide (ZnO) is a highly sought-after material for semiconductor applications. A II-VI semiconductor with a wide direct band gap (3.37 eV), ZnO emits light in the UV spectrum [1]. The large band gap means ZnO is transparent to visible light, making crystals colorless and clear. ZnO also has a high exciton binding energy (60 meV); with a binding energy higher than the average thermal energy at room temperature (25.7 meV) [2]. This high binding energy means that ZnO can emit bright light even at or above room temperature. ZnO's crystal structure is hexagonal wurtzite.

These characteristics make ZnO ideal for applications in optics, optoelectronics, and laser technologies. It is similar to the material gallium nitride (GaN), the most commonly used semiconductor for the UV range today, but has some distinct advantages over it. ZnO has a much higher exciton binding energy than GaN (25 meV), allowing for continued stability and use at higher temperatures [3]. Large single crystals of ZnO can be produced for much lower cost than GaN as well and can be used as a substrate for film growth. ZnO also lends itself to wet chemical etching, which is important for constructing semiconductor devices [5]. ZnO is highly resistant to damage from hard radiation, making it favorable for space applications [1]. The main reason ZnO is held back from being used in these technologies is the difficulty of growing viable p-type ZnO material. This work explores rf magnetron sputtering as a method for growing thin films of ZnO doped with arsenic (ZnO:As) to make them p-type.

1.2 **Doping**

Semiconductors can be made “p-type” or “n-type” depending on their electrical properties that arise from introducing different defects into their crystal structure. These defects are usually caused by replacing elements of the crystal lattice of the semiconductor with a different kind of atom. The new element must have a different valence from the original. “Valence” refers to the number of electrons in the atom that are used to form bonds with other atoms. If the element introduced has a higher valence than the one replaced, an extra electron is available that was not used in the bond. This electron becomes a charge carrier for the semiconductor. Since electrons are negatively charged, semiconductors that have this kind of defect are designated “n-type.” These defects are known as “donors,” because they “donate” electrons. If the element introduced instead has a lower valence than the original atom it is replacing, then there is one electron fewer in the bond, and a hole is formed. A “hole” is a quasiparticle that has the same mass as an electron, but a positive charge instead of a negative one. When this positively charged particle is the predominant charge carrier of a semiconductor, that semiconductor is designated “p-type.” These defects are known as “acceptors,” because they can “accept” electrons from an outside source.

Due to defects in its crystal structure ZnO is almost always n-type when grown. It is widely believed that the defects causing the material to be n-type are “native defects” (irregularities in the crystal lattice that occur during crystal formation), such as oxygen vacancies and zinc interstitials [2]. Other research suggests that because these vacancies and interstitials are deep donor defects (defects which do not produce charge carriers), external impurities, such as

hydrogen impurities, are the more likely cause [1]. In any case, the high amount of easily-created donors is largely why it is so difficult to achieve p-type ZnO.

To overcome the large number of donors present, a sufficient amount of p-type dopant must be added. This process is known as "compensation." Normally many different types of dopants are present in a given semiconductor, and the holes and electrons will cancel out to leave no free charge carriers if they are present in roughly equal amounts. However, in ZnO the possible native p-type defects (oxygen interstitials and zinc vacancies), which would potentially compensate for the native n-type defects mentioned above, have high formation enthalpy and are very unlikely to form [3]. Additionally, very few impurity atom candidates for shallow acceptors exist for ZnO, further hampering development of p-type material [3].

Traditional methods of introducing p-type dopants in semiconductors have proven ineffective for ZnO. The most common method of doping semiconductors is by molecular diffusion [4]. Due to the need to overcome the n-type defects and impurities, a lot of dopant must be added. ZnO has a low solubility for most acceptors, however, and does not remain stable when so much dopant is added [3]. For this reason, other methods of doping must be used.

1.3 **RF Magnetron Sputtering**

One possible method of doping ZnO is through rf magnetron sputtering (hereafter referred to as sputtering). Sputtering is essentially ripping bits of a material off of a bulk sample and depositing them somewhere else. Figure 1 shows a diagram of rf magnetron sputtering, which works by igniting a plasma, such as argon (Ar), and confining it to a small region on a cathode with an electrical signal. A radio frequency alternating current causes the ions of the plasma to cycle between attraction to and repulsion from the cathode. The material that is to be sputtered,

called the “target,” is placed in front of the cathode such that the plasma forms on its surface. A magnet located behind the target allows high-energy electrons to be trapped along its magnetic field lines; these trapped electrons sustain the plasma by continuously ionizing the Ar atoms. When attracted to the cathode, the ions run into the target with enough force to launch particles off of the surface. These particles travel until finding a new surface on which to deposit: the substrate placed at the bottom. As more and more particles land on the substrate, they form a thin film of the target material.

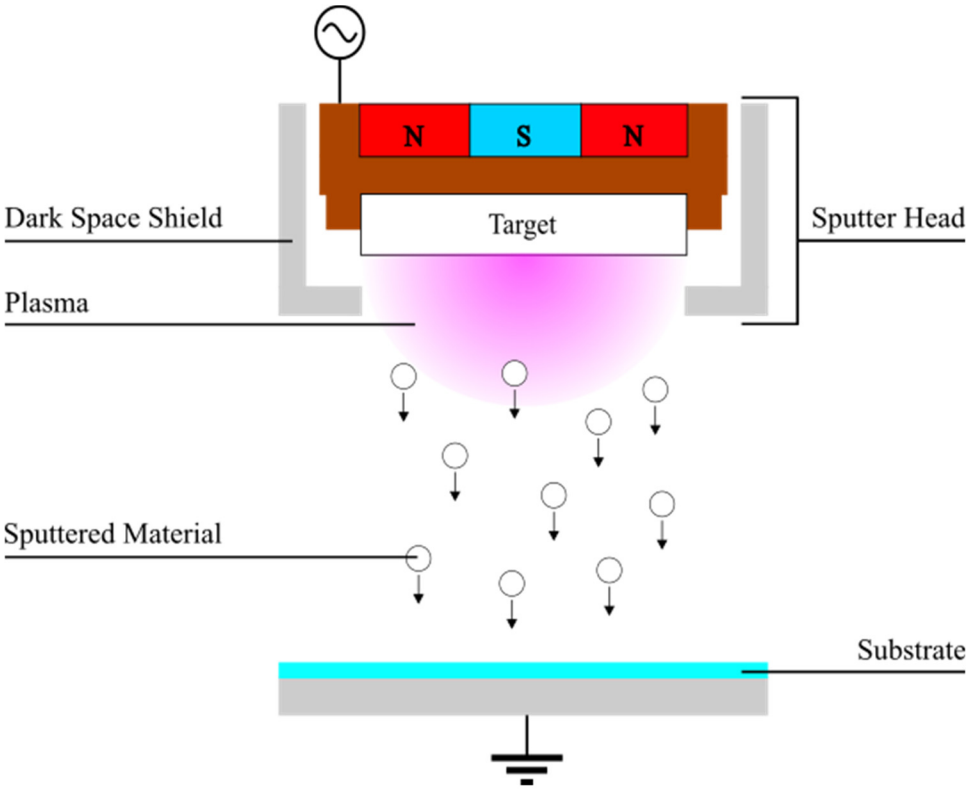

FIG. 1. Set-up of a rf magnetron sputtering chamber. A radio frequency electrical signal ionizes the gas in the chamber, which forms a plasma. The plasma is confined to the target surface by the magnet and the dark space shield. The plasma tears off particles of the target, which then deposit on the substrate below.

Sputtering allows us to add dopants between when the ZnO is sputtered and when it deposits on the substrate. We are pursuing using arsenic (As) to act as an acceptor and produce stable p-type ZnO. Our theory of the process, as conceived by Gary Renlund, is that the As atoms introduced attaches directly to the ZnO crystal lattice through a three-body collision, as shown in Fig. 2, in the atmosphere of the sputter chamber [6]. By heating the substrate, the As atoms previously deposited there become mobile enough to detach from the surface. When the As atoms meet the Zn and O atoms which are being sputtered, they have the opportunity to form bonds. If the As attaches to the Zn, the As makes it into the crystal lattice. Incorporating the As in this way prevents it from diffusing out, but still forms a shallow acceptor defect that produces a hole. If the As attaches to O, it forms a stable arsenic oxide gas (presumably As_2O_3) and is evacuated from the chamber instead of becoming a dopant [8]. We don't know for certain that this is the exact mechanism by which As is introduced into the crystal structure, but it has been verified that As successfully acts as an acceptor defect when incorporated into the ZnO by way of sputtering [7].

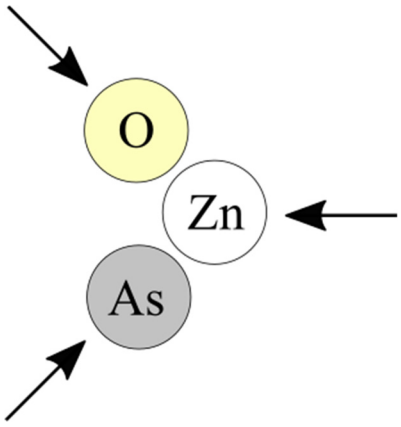

FIG. 2. Three body collision of arsenic, zinc, and oxygen. For the arsenic to be incorporated into the ZnO lattice it must combine with the zinc and not the oxygen while in the atmosphere of the sputter chamber.

1.4 **Previous Work**

Gary Renlund *et al.* used rf magnetron sputtering in the past to produce stable p-type ZnO [9][7]. This thesis uses his work as a basis. The samples produced by Renlund with this method have been confirmed p-type and have shown to hold their properties for years after their initial production. An analysis of the elements in the films, as a function of the depth of the film, is done by secondary-ion mass spectroscopy (SIMS). The result of their SIMS analysis is shown in Fig. 3 [9][7]. The line representing As shows that As is present throughout the film at a concentration between 10^{19} and 10^{20} cm^{-3}, suggesting this technique does manage to incorporate As into the ZnO films. The spike in concentration from 500-600 nm corresponds to the layer of Zn_3As_2. This gives us confidence that we can reproduce the p-type material grown in these experiments.

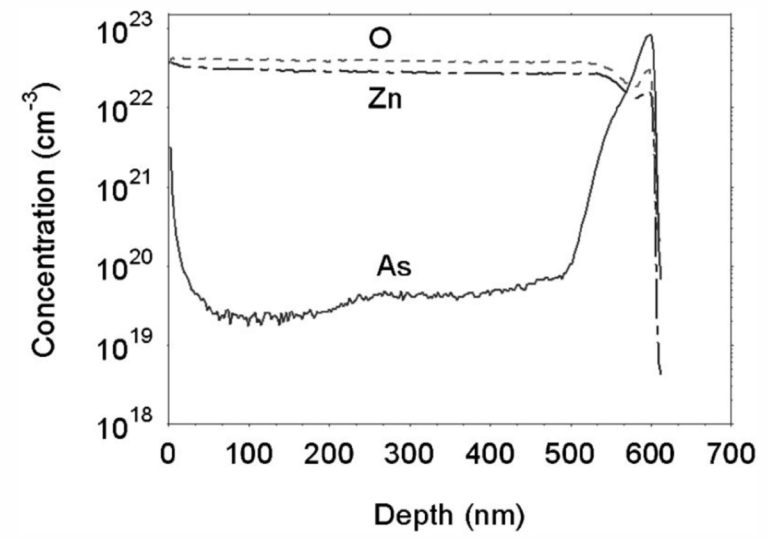

FIG. 3. SIMS analysis of Renlund *et al.* p-type ZnO samples. Arsenic is found both throughout the film, and underneath the ZnO film where the ZnAs layer was deposited. The concentration of As throughout the film is typical of a dopant. From Ref. [8].

1.5 **Overview**

The primary objective of this thesis is to report on our recent methods used to produce stable p-type ZnO. I start by detailing the techniques and parameters of the growth of our samples. I then move on to a description of the techniques we use to characterize the electrical and optical properties of our thin films, as well as the crystallinity. In each of these sections I provide an analysis of the results of these measurements. I end by discussing the overarching achievements of this research to this point and highlight the work that still needs to be done.

2 Methods

This chapter contains information regarding the growth parameters and practices used to create p-type zinc oxide by doping with arsenic through rf magnetron sputtering. A description of how to perform the characterization processes is also included.

Our method of doping ZnO with As is achieved through depositing a thin film via sputtering. We use a system of layers to allow the dopant to be introduced into the film, shown in Fig. 4. The following sections discuss the application of each layer.

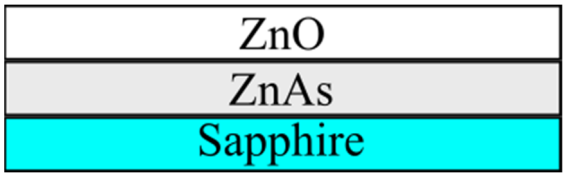

FIG. 4. Layer model. We first deposit zinc arsenide, our source of dopant, on top of our sapphire substrate. The zinc oxide is then sputtered directly onto the ZnAs layer.

2.1 ZnAs Layer

We start by evaporating zinc arsenide (Zn_3As_2, referred to as ZnAs from here on out) onto c-plane cut sapphire wafers in a Denton evaporation chamber. We have also deposited on fused silica and glass as substrates, but sapphire has produced the best results (see section 5.3 later in this thesis). Inside the chamber, we put ZnAs powder in a graphite crucible. The crucible is surrounded with a coil of tungsten wire that heats it up. The chamber is evacuated using a turbomolecular vacuum pump to a pressure of about 1×10^{-5} torr. We run a current through the wire to heat up the crucible. The current is controlled with a Variac variable transformer. The

Variac draws a standard 120 V from the wall and transforms it into DC current. We set the transformer to allow 60% of the full scale power through the wire. Evaporating under these conditions for 60 s allows for a layer of ZnAs (20-70 nm in thickness) to be deposited on the sapphire wafers. A more comprehensive study of the ZnAs layers is explored in the thesis of Colter Stewart [11].

2.2 **ZnO Layer**

In order to sputter a layer of ZnO we need a sputter target. We press a target following instructions from Gary Renlund [10]. The target is made by pressing and firing ZnO powder (99.999% purity). See Ryan Peterson's senior thesis for more details on the composition of the target [11]. The powder is mixed with Duramax B-1000 binder in a mortar and pestle. Once it reaches the proper consistency, the powder-binder mixture is pressed into a target using a 2" diameter steel die. The target needs to be 1" in diameter, so a 2" die is used to allow for shrinkage during firing. A hydraulic press on BYU campus is used to reach 3.75 tons while pressing the target. Afterwards the target is fired in a kiln at 1100 ℃, which Gary Renlund did for us at his house, to solidify the target and burn off the binder so that it does not contaminate the films. The target is then sanded down to be 1" in diameter using a grindstone in the machine shop of the Eyring Science Center. Finally, one side of the target is sanded (using sandpaper) to be flat.

Once prepared, the target and substrate are placed in the sputter chamber (see Fig. 1). The target is placed in the 1" metallic sputter head at the top of the chamber with the sanded side flush to the surface of the head and the un-sanded side pointing towards the bottom of the

chamber. An aluminum dark space shield covers the head and is adjusted to have a 3 mm separation from the surface of the target. The wafer with the ZnAs layer is then placed near the center of the steel substrate heater below the sputter head, and the chamber is closed.

The chamber is then evacuated as low as the vacuum system allows. Typically we sputter while in the 10^{-6} torr range. To achieve this pressure we use a roughing pump to reduce the pressure in the chamber to the 10^{-3} torr range, followed by a turbomolecular pump that allows the chamber to be evacuated to the 10^{-6} torr range. Once the chamber is evacuated, the substrate heater is turned on and heated to typically 650 °C. The walls of the chamber and the interior of the sputter head are kept cool by running water through tubes surrounding them. This prevents warping of the metal (and subsequent vacuum leaks) and damage to the electronics due to the high temperatures.

Once the chamber reaches the required conditions, the rf electrical signal is then turned on. The rf signal is controlled via a Seren rf automatic matching network. The matching network has two capacitors that control the signal: a “load” capacitor and a “tune” capacitor. When the rf signal travels through the network, power can be reflected and travel backwards. These capacitors are adjusted to minimize reflected power through the system. Our sputtering was typically performed with 75 W forward power and zero reflected power until we encountered some system failures. After getting the sputter system back online we now sputter with about 20 W reflected power and 75 W forward power. Once the rf signal is stable, argon and oxygen gas are introduced into the chamber. A flow rate controller regulates the amount of gas allowed into the chamber. We found 10 cc/min of O_2 and 80 cc/min of Ar to be optimal for sample growth. However, in order to strike the plasma a “surge” of Ar gas is needed, after which 80 cc/min is sufficient to maintain the plasma. This surge of Ar is achieved by opening the Ar flow controller

valve after setting the flow rate to 80 cc/min, as opposed to opening the valve and slowly bringing the flow up to 80 cc/min.

The plasma, once struck, should be a light purple color and cone shaped, extending about 2 inches off of the target surface. The plasma should be confined to the surface of the target by the dark space shield. If the target is not sufficiently clean, some sparking can be observed on its surface which, though not harmful to the target, may indicate surface contamination. In such a case, we sputter until the sparking stops, at which point the target is clean. Typical pressures in the chamber during sputtering are in the 10^{-4} torr range. The time spent sputtering may be adjusted to grow films to the desired thickness, and the majority of our samples were grown for either 30 or 60 min. When the desired time elapses, the rf power is turned off and the gas flow valves closed. The heater is then powered down and the chamber vented to allow it to be opened and the sample retrieved.

2.3 **Annealing**

The films can then be annealed to help improve crystal structure and optical properties. Annealing refers to the relaxation that the crystal structure undergoes when the film is slowly heated and then slowly cooled. By gradually adding energy into the bonds between the atoms in the crystal, they are able to "shift" into the configuration with the lowest energy state. This corresponds to the most ordered crystal structure possible, which displays the best properties. A tube furnace is used to reach the appropriate temperatures while controlling the atmosphere. We place the sample inside of a quartz tube, which we evacuate with a turbomolecular pump to 10^{-6} mBar (about 0.75×10^{-6} torr). The furnace is programed to rise to 750 ℃ over 4 hrs, remain there

for 2 hrs, and then cool back down over 6 hrs. These values were chosen at the suggest of Gary Renlund to allow the temperature to slowly rise and fall.

After these steps are completed, we have created a thin film of ZnO that is doped with As which need to be characterized to determine the electrical, optical, and crystal properties of the sample.

3 Electrical Properties

To determine whether the ZnO films we have deposited are p-type, we examine the electrical properties of the films. This chapter discusses the electrical properties of the films we investigate with Seebeck and Hall effect measurements. Our understanding of the factors that affect the measured properties are discussed.

3.1 Seebeck Effect

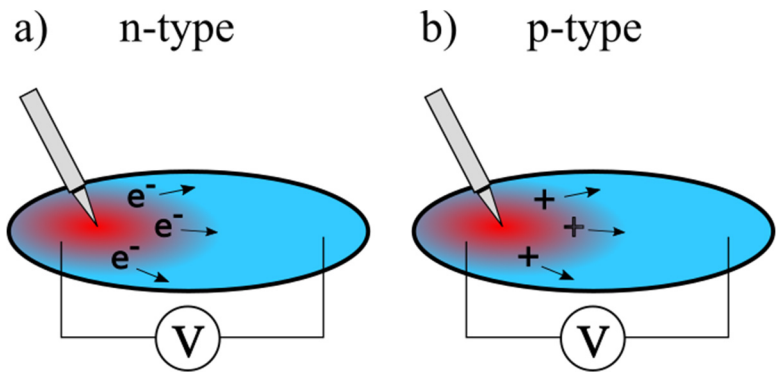

FIG. 5. The Seebeck effect. When heated, the charge carriers in the region move away from the heating source, creating a voltage across the surface. The charge carriers in a) n-type material are electrons, and in b) p-type material are holes. The sign of the voltage tells us which kind of charge carriers we have.

The Seebeck effect is the direct conversion of heat to electricity, and occurs when we heat up the surface of our films [14]. The heat transfers to the charge carriers, which convert it to kinetic energy. By heating a select area, only the charge carriers in that area gain energy. The charge carriers undergo thermal diffusion and move away from each other and from the point at

which thermal energy is being added. This motion creates a net voltage between the point where heat is transferred and the surrounding parts of the film.

We use the Seebeck effect to quickly determine whether the films are p-type or n-type, giving an immediate measure of the success of the film deposition. As shown in Fig. 5, a voltmeter is used to measure the voltage across the sample surface over a distance of about 1 cm. The positive probe is touched to the surface while the negative probe is attached to a hot soldering iron. When the hot probe touches the surface, the charge carriers gain energy and move away from the probe. If the charge carriers are holes (positively charged), this movement creates a net positive charge at the positive lead, and the voltage reads positive: a positive voltage signifies that the film is p-type. If the charge carriers are electrons (negatively charged), then the opposite happens and a net negative voltage is measured: the film is determined to be n-type.

3.2 **Hall Effect**

The Hall effect occurs when a current is run through our film in the presence of a magnetic field. This magnetic field produces a Lorentz force that acts on the individual charge carriers and causes them to move to perpendicular to both the magnetic field and the direction of the current (the electric field). This movement creates a transverse voltage across the sample, which can be measured to determine the type of charge carriers in the film. By repeating this experiment across the different dimensions of the sample, the carrier concentration (charge carriers per unit volume) and mobility (conductivity per charge carrier concentration, divided by e) can also be determined. This way of measuring the Hall effect is known as the Van der Pauw

method [15]. The carrier concentration and mobility determine how well the semiconductor is able to conduct electricity.

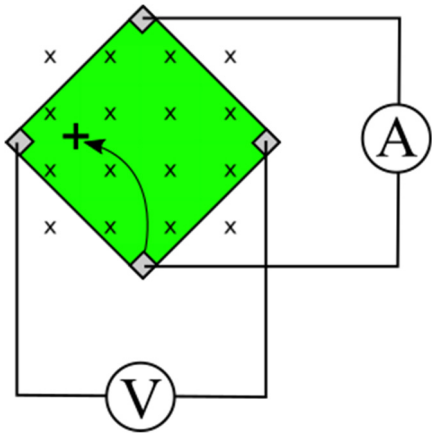

FIG. 6. Van der Pauw method for measuring the Hall effect. Using a square-shaped sample, a current is run through the material at its corners while a magnetic field is applied perpendicularly to the surface. By measuring the voltage across the sample, we can determine the electrical properties of the material. Repeating the measurement while rotating which corners are used to conduct the current gives us more accurate values for these properties.

In order to determine these characteristics of our films, we use the van der Pauw method with the apparatus shown in Fig. 6. The films must be cut into a square shape to get an accurate measurement. Indium placed on the corners improves electrical contact between the leads and the sample surface. The film is placed on the apparatus, with the electrical leads placed on the indium on each corner. We send a current in the nano-amp range through the sample across two of the leads. The voltage is measured across the other two leads without a magnet in the apparatus, then with a 0.51 T magnet oriented with the north side on top of the sample, and finally with the magnet's south side on top of the sample. The magnet causes the charge carriers to deflect towards one of the other leads, regardless of what kind of charge carriers are present, creating a voltage across the leads that do not have the current applied to them. This process is repeated four times—cycling through each opposing pairs of leads. From these voltages the computer determines and records the properties of the film.

3.3 **Results**

A complete chart of our samples, alongside their sputtering conditions and electrical results, can be found in Appendix A. The general trends in the data are discussed here. The majority of the films we made have been n-type, but the most recent ones have been confirmed p-type. Since reducing the concentration of oxygen in the plasma, the majority of the samples have come back p-type. Carrier concentration and electrical resistance have varied wildly from sample to sample. The best sample we have ever produced (sputtered 5/14/18 on sapphire) shows carrier concentrations on the order of $p = 10^{20}$ cm^{-3} and resistance as low as 500 Ω. The others have had a carrier concentration as low as $p = 10^{16}$ cm^{-3} and resistance up to 150 kΩ. We have not been able to determine what exactly causes these fluctuations, and more study is needed.

Despite the inconsistency of the electrical properties in the films produced, we have been able to confirm their stability (i.e. they remain constant over long periods of time). Measurements of their electrical properties taken more than six months after the initial production of the films have shown little to no variation from the original values.

4 Optical Properties

ZnO is sought after for its ability to emit light in the ultraviolet range. Measuring the spectrum of light that our samples emit allows us to know how well the produce they band edge emission (the highest energy light they can produce), and what kinds of defects are present in the material. This chapter discusses the optical measurements that we perform on our films, and the sputter parameters that those measurements have helped us optimize.

4.1 Photoluminescence

Photoluminescence (PL) measurements are performed by collecting the light produced by the sample when excited by a laser. We gain information about the energy band structure and defect structure of the films by looking at the amount of light given off at different wavelengths. A comprehensive study of the PL of our ZnO films can be found in Ryan Peterson's senior thesis [13]. In PL measurements, the samples are typically placed in a cryostat and cooled to a temperature of 15 K. They are then illuminated by 266 nm wavelength light from a pulsed, frequency tripled Ti:Sapph laser. This light is much higher energy than the band gap of ZnO. Using high energy light allows all of the energy levels in the film to be excited and emit light, and the laser's wavelength will not overlap with those of the emitted light. The light produced is collected and focused into a JY Horiba Triax 5000 spectrometer. The spectrometer separates the light by wavelength and focuses them onto a JY Synapse CCD detector, which then reads the intensity of the light at each wavelength. The spectrum data for each sample is recorded by a computer into a spreadsheet for future analysis.

4.2 **Parameter Refinement**

Through analyzing PL data we were able to refine several different sputtering parameters, namely the sputter time, rf power, and gas concentrations used to sputter. We were also able to identify and eliminate certain defects that caused large amounts of PL in the visible spectrum.

4.2.1 Sputter Time

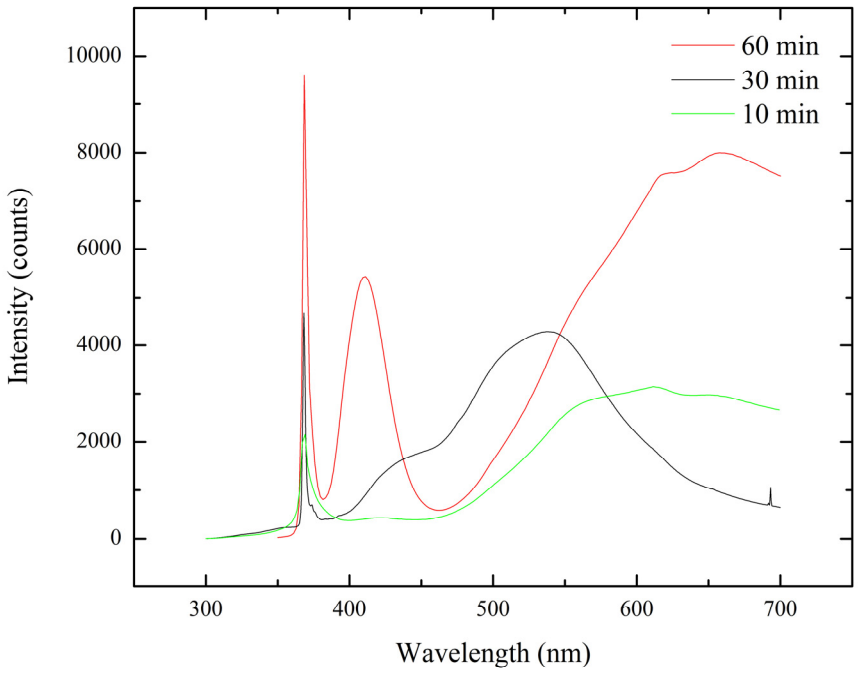

FIG. 7. ZnO PL spectra comparing sputter time. Longer times spent sputtering result in more band edge PL.

We varied the time spent sputtering at 75 W from 10-60 min to see if it affected the PL produced. PL measurements of these samples (samples ZnO-180217B, ZnO-180217A, and ZnO-180217C in Appendix A) are shown in Fig. 7, and show that longer times correspond to higher band edge emission (370 nm). The films are thin enough that the laser light passes through them completely, and sputtering for longer periods creates thicker films. Increasing the thickness would account for the increase in the emission without necessarily improving the quality of the

samples. This is supported by the 60 min run band edge PL being nearly twice the height of the 30 min run band edge PL. The variation in the visible spectrum PL, however, suggests different defects may occur at different times during sputtering. More study would be needed to investigate the causes of this, but was not our primary concern for this particular study.

4.2.2 RF Power

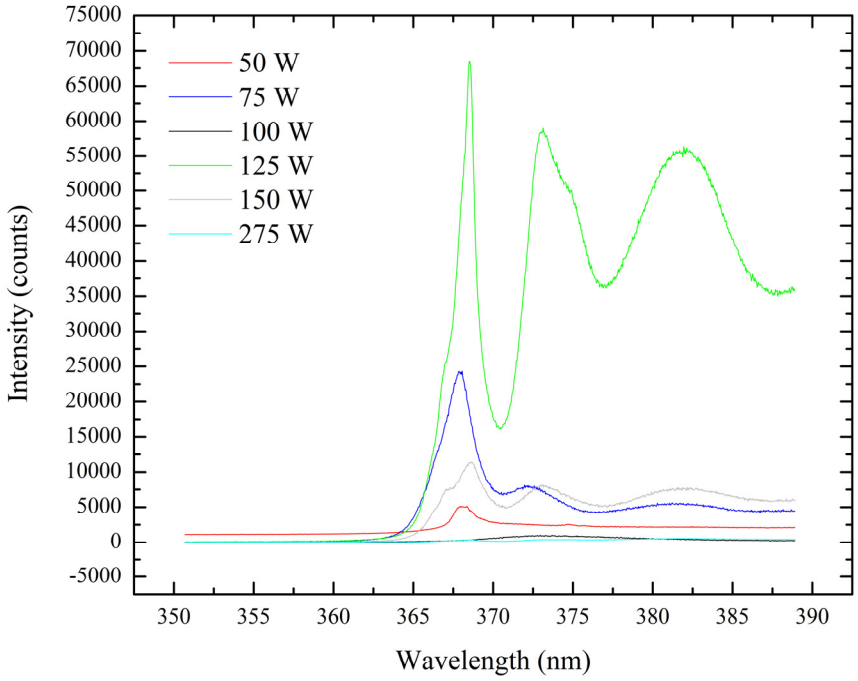

FIG. 8. ZnO PL spectra comparing rf powers. The different spectra were taken under the same conditions, and we expect their relative intensities to be indicative of how well each sample was emitting PL at the band edge.

To find the optimal rf power for sputtering, we varied the rf power used to sputter from 50-275 W, sputtered for 30 min each (samples ZnO-170815A, ZnO-170815B, ZnO-170815C, ZnO-170823B, ZnO-170830B, and ZnO-170830A in Appendix A), and observed the resulting PL spectra, shown in Fig. 8. The data shows that we got the most band edge PL when sputtering at 125 W. Despite this result, we settled on sputtering at 75 W to minimize the strain on the

sputter system without sacrificing too much PL. Going forward it will be interesting to see if sputtering at 125 W significantly improves other qualities of the ZnO films.

4.2.3 Gas Concentration

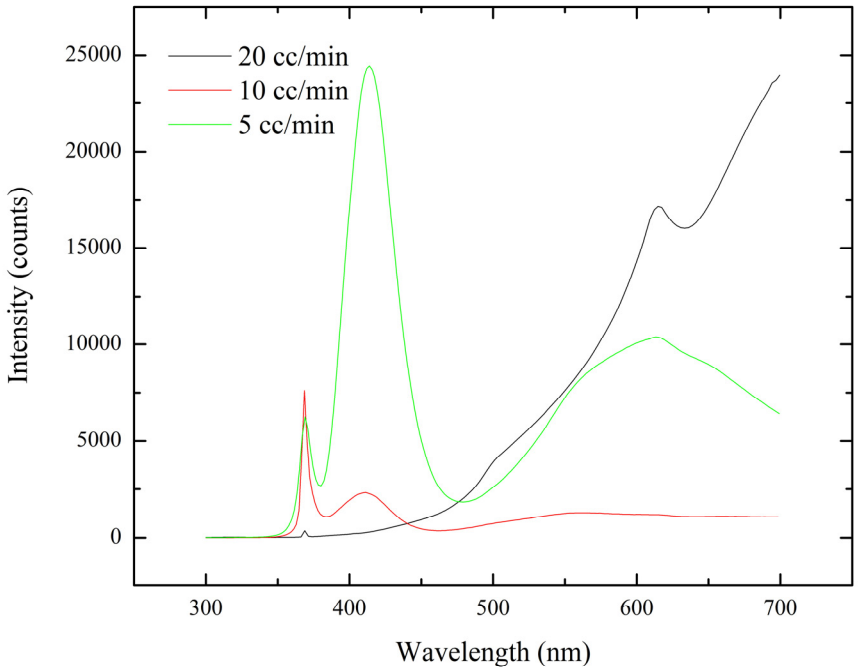

FIG. 9. ZnO PL spectra comparing O_2 concentrations. 20 cc/min (black) is the concentration that we sputtered at for the majority of our runs until varying this parameter.

The plasma gases used were Ar and O_2. Varying the flow rate of Ar did not produce films with any different qualities, so we used 80 cc/min as it produced a strong plasma. Varying O_2 flow from 5-20 cc/min with 30 min sputter time and 75 W rf power (samples ZnO-180502A, ZnO-180502B, and ZnO-180405 in Appendix A), however, had a strong effect on the results, as shown in Fig. 9. Lowering the flow rate to 10 cc/min decreased the huge amounts of visible PL present in our films, as well as significantly affecting our ability to produce p-type material. Decreasing the flow rate further brought different defects to prominence, as seen by the vastly different spectrum produced. Our hypothesis on outset was that stable doping with As is

achieved through a three-body collision in the atmosphere between As, O, and Zn. Changing the amount of O_2 gas may have been necessary to reach the conditions under which these collisions are more likely to occur.

4.2.4 Dark Space Shield

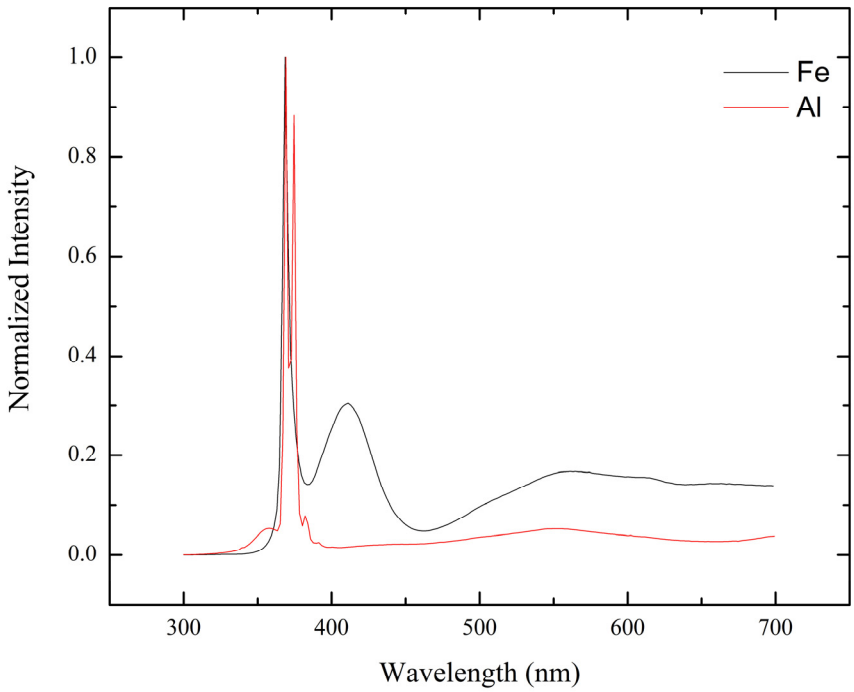

FIG. 10. ZnO PL using Al and steel dark space shields. PL comparison of aluminum (red) and stainless steel (black) dark space shields. Each curve has been normalized to better show the relative heights of the peaks. Switching to the Al dark space shield eliminated the iron peak at 410 nm as well as the majority of the remaining visible PL.

The original dark space shield that came with the system was made of stainless steel. While sputtering with this dark space shield, we noticed a peak on the PL spectrum at 410 nm. Investigation led us to believe that this peak may have been caused by the introduction of either iron (Fe) or aluminum (Al) as a dopant in our films [16]. To prevent Fe from contaminating our ZnO films we switched from the stainless steel darks space shield to an Al dark space shield, made at the BYU machine shop. Examining the PL spectra produced by the films deposited with

the Al shield (samples ZnO-180502A and ZnO-180612B in Appendix A), shown in Fig. 10, we find that the 410 nm peak disappears from our PL spectrum. This result leads us to believe that the 410 nm peak is caused by unintentional Fe doping. The Fe contamination may be caused by the plasma not being completely confined to the surface of our target, and potentially means that we are now adding Al into the film in place of Fe. Additional tests are needed to confirm whether we are now contaminating our samples with Al.

5 Crystal Structure

This chapter discusses the methods we use to determine the crystallinity of our films, and the implications of their results.

5.1 X-ray Diffraction

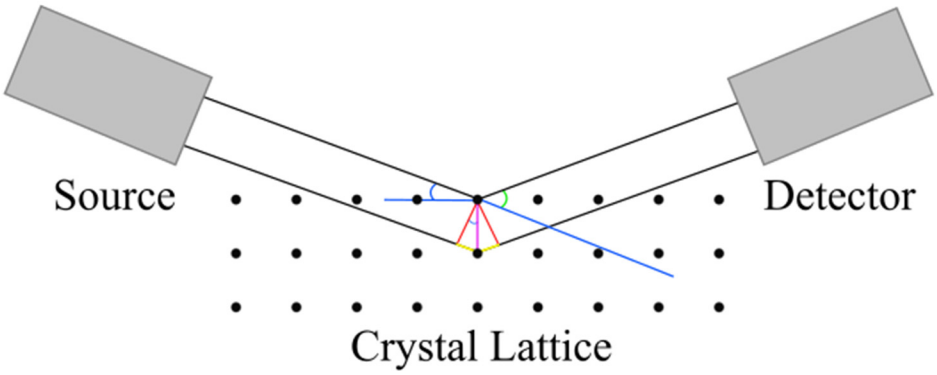

FIG. 11. X-ray diffraction schematic. The condition for diffraction is given by Bragg's law (2), and requires that the yellow section be equal to an integer number of wavelengths of the x-ray. The blue arc is the angle at which the x-rays enter, and the green angle is the position at which they leave, known as 2θ. The pink line is the crystal spacing.

X-ray diffraction (XRD) allows us to determine the crystal structure of our films, leading to insights about defect structure, and confirming production of ZnO. XRD is a technique in which x-rays are sent into a crystal, and the diffraction pattern that results is used to determine the ordering of the atoms in the crystal, known as the crystal lattice. Diffraction occurs according to Bragg's law:

$$n\lambda = 2d \sin\theta \tag{1}$$

which describes the condition for which the diffracted x-rays constructively interfere. Bragg's law says that the x-rays that diffract off of different crystal planes only constructively interfere if the path length difference is an integer n times their wavelength λ. This only occurs when the

spacing between crystal planes *d* times the sine of the incident angle θ of the x-rays is also equal to an integer number of x-ray wavelengths. XRD measurements work by measuring the angle 2θ at which constructively interfering diffracted x-rays are found.

A PANalytical X'pert Pro MPD diffractometer is used to perform these measurements. The films are placed in a zero-background sample holder with double sided tape to hold them in place. The sample height is adjusted so that the film surface is flush with a glass slide placed across the top of the sample holder. This configuration places the sample at the correct height for the measurement to be accurate. The sample is then placed into the diffractometer. Diffraction data is taken using 0.04 rad soller slits (which keep the beam collimated), the largest mask that allows the beam to cover the sample without spilling off the edges of it (usually 15 mm), and automatic diffraction slits to account for the effective sample depth changing at different angles of measurement. A current is run through a filament, causing electrons to be fired from the filament. The electrons experience a voltage, which propels them towards a block of copper. The electrons strike the copper and produce characteristic x-rays with a wavelength of 0.154 nm [17]. The x-rays are then directed into the sample, where they diffract. Diffraction data is measured over the angles $2\theta = 20°$ to $80°$ over several hours. This results in a list of diffracted intensities as a function of incident angle.

5.2 **Deposition Temperature**

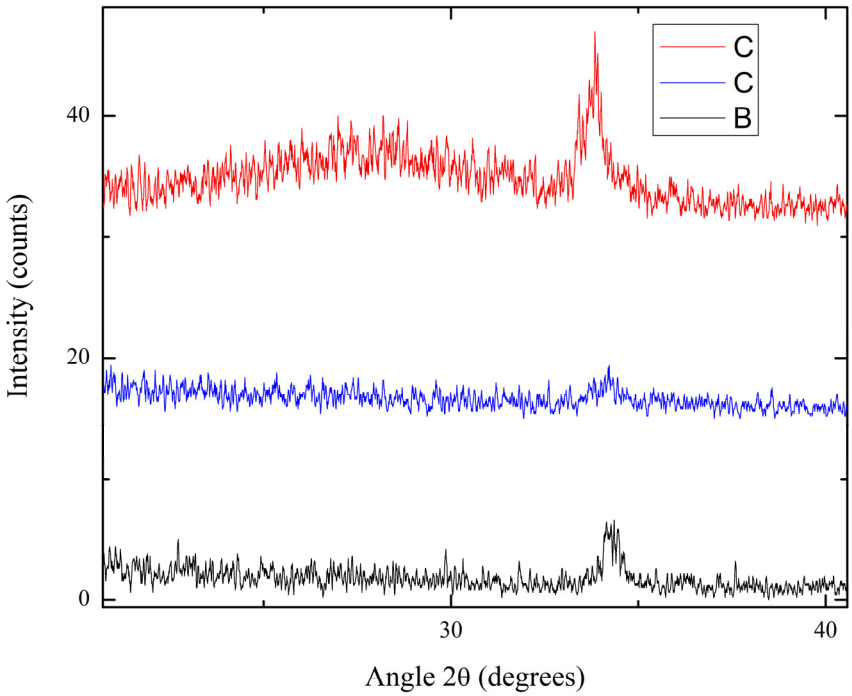

FIG. 12. ZnO XRD pattern comparing substrate temperature during growth. These samples were not annealed. The highest temperature yielded the best XRD pattern, though no other parameters were optimized yet so the effects are hard to observe.

We varied the substrate temperature while sputtering from 400 °C to 650 °C (samples ZnO-180214A, ZnO-180214C, and ZnO-180217A in Appendix A). The XRD data in Fig. 12 shows that the highest temperature gave us the most diffraction. The differences between the patterns are minimal, most likely due to no other parameters being optimized at this point. Repeating this test now that other parameters have been optimized may be worthwhile. We are limited from investigating higher temperatures by the safe operating temperatures of the heating element in the sputter chamber: the temperature cannot exceed 650 °C.

5.3 **Lattice Matching**

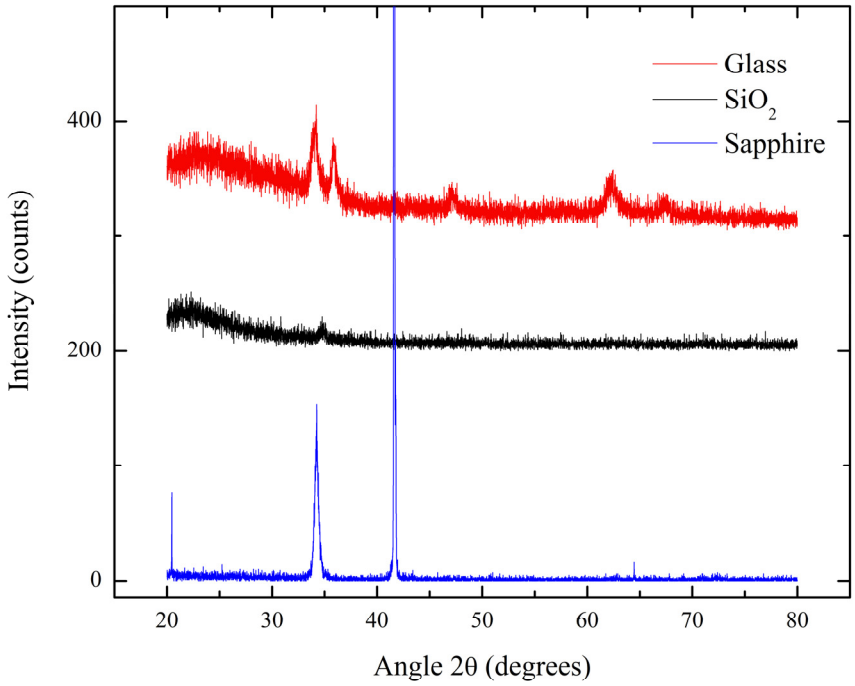

FIG. 13. ZnO XRD pattern substrate comparison. A comparison of the crystallinity of ZnO deposited on glass (red), fused silica (black), and sapphire (blue), offset for comparison. Sapphire shows the most crystalline pattern, having the narrowest, and most intense, peak at 2θ = 34.5º which corresponds to ZnO.

The crystal structure of the substrate has a significant effect on the crystal quality of the films being grown. To find an appropriate substrate, we sputtered onto 3 different materials: glass, fused silica (SiO_2), and c-plane sapphire wafers (Al_2O_3). Despite having an intermediary layer of ZnAs, the effects of the substrate on the ZnO layer are still visible. We determined that sputtering onto sapphire was most favorable due to the improvement of the crystallinity of the films. The x-ray diffraction (XRD) data in Fig. 13 (samples ZnO-170921A, ZnO-170921B, and ZnO-170503A in Appendix A) shows that the sharpest peaks produced came from samples sputtered on top of sapphire, while silica and glass both became highly amorphous. The amorphousness of glass and silica is seen by the wide hump on the left side of their patterns. This

is confirmed by the relative height of the band edge photoluminescence (PL) produced by films sputtered on sapphire being higher than that of the other substrates.

5.4 **Annealing Results**

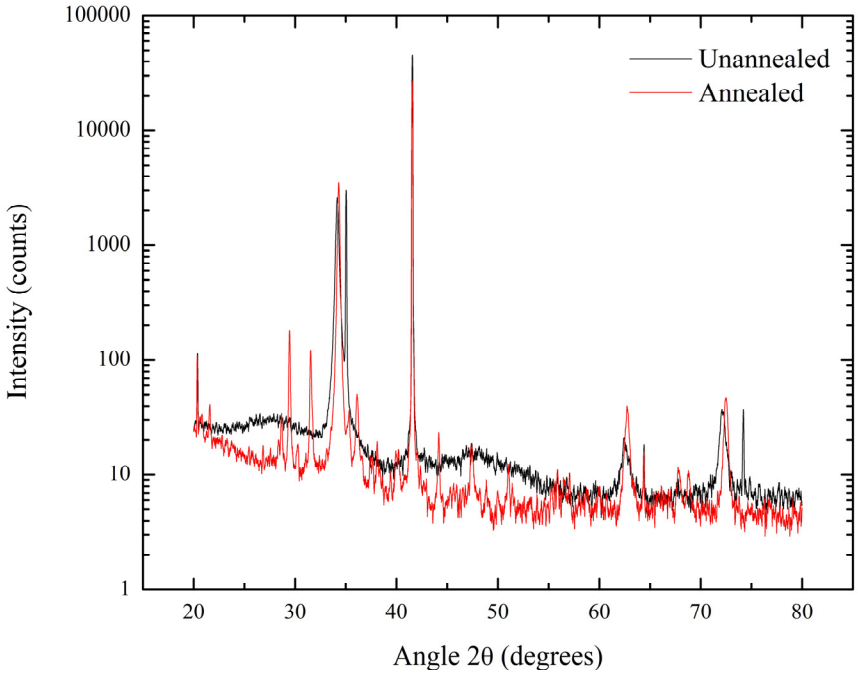

FIG. 14. XRD pattern for ZnO before and after annealing. These samples were deposited on sapphire and then annealed. In addition to many peaks resolving after annealing, the peaks at 34°, 62°, and 72° 2θ show reduced FHWM**.** The peaks at 2θ = 20° and 41° are from the sapphire substrate and can be ignored.

As discussed previously, annealing is a technique used to improve the crystallinity of our films by letting them relax into a lower energy configuration. The data in Table 1 shows that the full width at half max (FWHM) of the peaks of the XRD patterns shown in Fig. 14 (sample ZnO-170907B in Appendix A) decrease after annealing, suggesting the material becomes more crystalline. Many peaks that are not well resolved before annealing also come into view after doing so. This is shown in that the humps in the unannealed graph (black) match up with the clusters of smaller peaks on the annealed graph (red).

Table 1. Reduction in XRD peak FWHM due to annealing. Annealing the ZnO improves its crystallinity, as evidenced by the reductions in FWHM over 50% for each peak in the XRD pattern. All units are in degrees.

Angle 2θ	Unannealed FWHM	Annealed FWHM	% Decrease
34	0.27	0.17	62
62	0.72	0.39	54
72	0.66	0.35	53

5.5 **Crystal Domains**

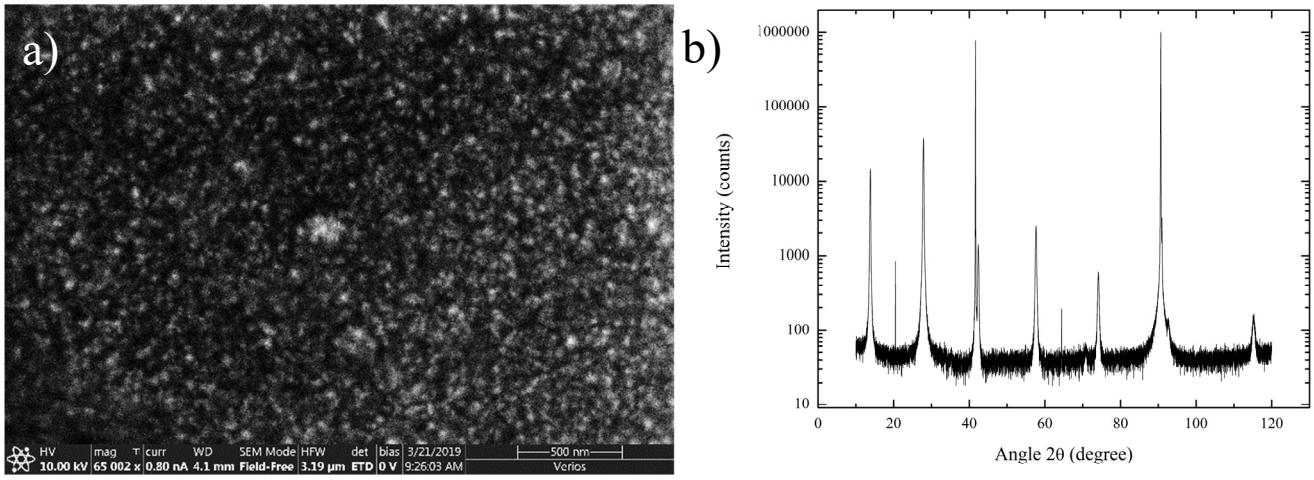

FIG. 15. ZnO Crystallites. The size of the crystallites seen in a) the SEM image of the sample are related to the FWHM of the peaks in b) XRD pattern by Scherrer's equation (2).

Recent scanning electron microscope (SEM) imaging of our films (sample ZnO-180502B in Appendix A) shows that, far from being single crystal, our sample surfaces are made up of randomly aligned crystallites. By using the Scherrer equation:

$$\tau = \frac{K\lambda}{\beta \cos\theta} \tag{2}$$

which relates the diamter of particles, τ, smaller than one μm to the broadening of peaks in a diffraction pattern, we can determine the sizes of these crystallites. The variable K is a dimensionless shape factor (roughly equal to 0.9 for our purposes, due to our nanoparticles being spherical), λ is the wavelength of the x-rays, β is the full width at half max of the peaks in the XRD data, and θ is the angle at which the peak is located [18][19]. The XRD data is plotted against 2θ, so the angle taken from the data must be divided by two. Analysis of the data in Fig. 15 shows that the crystallite sizes for this sample are between 30-50 nm in diameter.

5.6 Zn_3As_2 Structure

The Zn_3As_2 (referred to as ZnAs throughout this thesis) layer that supplies the As that dopes our films is a key parameter to producing p-type ZnO films. Unfortunately, not much research has been done on ZnAs itself. We have begun looking into the crystal structure of ZnAs in order to improve our production of ZnO:As.

ZnAs is believed to have a similar structure to Cd_3As_2, which is shown by Steigman and Goodyear to have a 75% cation deficient anti-fluorite [17]. Applying this structure to ZnAs means that there are ordered Zn vacancies throughout the crystal. The space group that ZnAs occupies given these assumptions is $I4_1cd$ (110), the same as Cd_3As_2. However, consulting with Branton Campbell leads us to believe that ZnAs actually belongs to the space group $I4_1/acd$ (142), which has higher symmetry [20]. This takes into account the 4×2×2 superlattice that is measured by Cole, Chambers, and Dunn, which results from displaced atoms in the crystal structure [19].

6 Conclusions

This thesis has investigated rf magnetron sputtering as a method to produce stable p-type ZnO:As. Films of ZnO were sputtered on top of a layer of ZnAs to allow dopants to enter the crystal structure. The electrical and optical properties, as well as the crystallinity of the films were evaluated. Seebeck measurements have verified the production of p-type ZnO thin films. Hall measurements have shown that high carrier concentrations can be produced with our method. Subsequent Hall measurements have confirmed that these carrier concentrations remain constant over long periods of time. Analysis of the photoluminescence and x-ray diffraction patterns of the films has allowed us to increase the band edge PL they emit and eliminate defects in the crystal structure.

From these results we conclude that rf magnetron sputtering can produce stable p-type ZnO:As thin films.

6.1 Future Work

Though out research group has produced p-type ZnO:As with increasing frequency, the exact conditions necessary for its production are still not clear. A highly conductive sample with our highest carrier concentration was produced early in the process, before systematically finding the parameters that allowed us to deposit p-type films with regularity. Attempts to reproduce the characteristics of this sample have been inconclusive. Recreating the conditions used for growing this sample has been insufficient to reproduce its properties, so one or more other variables is probably at play that must be uncovered.

Thus far, the factor that seems to have the strongest effect on the production of p-type material is the gas concentration used to form the plasma during sputtering. Since gas concentration is the parameter studied most recently, it is unclear whether the other parameters discussed in this thesis have more optimal settings for the gas concentration that we are now using. A study of the other parameters under this gas concentration may be useful to try and pinpoint the factors that control the electrical properties of the films.

By switching to an Al dark space shield, we possibly have begun to co-dope our films with both As and Al. A deeper analysis of our film composition and band structure may be able to answer this concern conclusively. The use of inductively coupled plasma ion mass spectroscopy (ICP-MS) and secondary-ion mass spectroscopy (SIMS) may be useful for discovering whether this defect is present.

Due to a lack of understanding of the ZnAs layer underneath our films, we have not been able to determine their exact thickness. Efforts are being made to characterize ZnAs with the hope that we will be able to measure our films through ellipsometry. This study will also allow us to control for the thickness of the ZnAs layer, and observe how it affects the properties of our ZnO layer.

Throughout this study, two different evaporators were used to form the ZnAs layers: one supplied by Gary Renlund, and one from David Allred. The analysis of the ZnAs layers done by Colter Stewart was on samples evaporated in the Allred evaporation system. Recently we have observed that the p-type samples produced were deposited on ZnAs that was evaporated in the Renlund evaporation system. We suspect this is due to the Renlund system being able to deposit thicker films, but a more in-depth analysis of the ZnAs layers is needed.

Appendix A

Table of the electrical properties of our samples. The green rows mark the p-type samples. An “x” in a cell means that a measurement was not able to be taken.

Sample	Substrate	Dark Space Shield	Substrate Temp (C)	Sputter Time (min)	Forward RF Power (W)	Gas Flow (cc/min)		Annealed?	Resistance (Ω, over 1cm)	Seebeck	Hall Measurements Carrier Concentration (cm^{-1})	P-type or N-type
						O2	Ar	Max Temp (C)				
Cermet ZnO crystal	None (solid crystal)	Steel	-	-	-	20	80	No	x	x	x	x
ZnO-170328	SiO2	Steel	400	30	75	20	80	No	inf	x	x	x
ZnO-170330	SiO2	Steel				20	80	No	x	x	x	x
ZnO-170414A	SiO2	Steel				20	80	No	200k	Convincingly p-type, data from 9-19-17	p-type (3E17)	p
ZnO-170414B	SiO2	Steel	475?	30?	75?	20	80	No	inf	x	x	x
ZnO-170418A	SiO2	Steel	475?	30?	75?	20	80	No	400k	Convincingly p-type (data from 9-19-17)	Type inconclusive (varied between p and n) Concentration ~10^16 **data from 1/25/18 stayed p-type, ~2-3E16**	p
ZnO-170418B	SiO2	Steel				20	80	No	x	x	x	x
ZnO-170503A	SiO2	Steel	525	30	75	20	80	No	300k	P-type	x	p
ZnO-170503B	SiO2	Steel	475	30	75	20	80	No	x	x	x	x

ZnO-170503C	SiO2	Steel	475	30	75	20	80	No	200k	N-type	x	n
ZnO-170504A	Microscope Slide	Steel	475	30	75	20	80	No	inf	x	x	x
ZnO-170504B	Al2O3	Steel	475	30	75	20	80	No	inf	x	x	x
ZnO-170504C	Zirconia	Steel	525	30	75	20	80	No	x	x	x	x
ZnO-170526A	Al2O3	Steel	475	30	75	20	80	No	x	x	x	x
ZnO-170624		Steel				20	80	Yes	x	x	x	x
ZnO-170526B	Al2O3	Steel	500	30	75	20	80	No	x	x	x	x
ZnO-170626		Steel				20	80	Yes	x	x	x	x
ZnO-170608A	SiO2	Steel	550	30	75	20	80	No	inf	x	x	x
ZnO-170608B	SiO2	Steel	550	30	75	20	80	No	1.4M	N-type	x	n
ZnO-170609A	SiO2	Steel	550	30	75	20	80	No	inf	x	x	x
ZnO-170609B	SiO2	Steel	550	30	75	20	80	No	300k	n type	x	n
ZnO-170616A	SiO2	Steel	550	30	75	20	80	No	x	x	x	x
ZnO-170616B	SiO2	Steel	575	30	75	20	80	No	100k	N-type	x	n
ZnO-170616C	SiO2	Steel	575	30	75	20	80	No	80k	n type	x	n
ZnO-170616D	SiO2	Steel	575	30	75	20	80	No	inf?	x (but open for debate I suppose)	x	n
ZnO-170616E	SiO2	Steel	600	30	75	20	80	No	x	x	x	x
ZnO-170623A	Glass	Steel	575	30	75	20	80	No	x	x	x	x
ZnO-170623B	Glass	Steel	575	30	75	20	80	No	inf	x	x	x
ZnO-170623C	Glass	Steel	575	30	75	20	80	No	inf?	x	x	x
ZnO-170623D	Glass	Steel	575	30	75	20	80	No	x	x	x	x
ZnO-170706A	Al2O3	Steel	575	30	75	20	80	No	inf	N-type	x	n
ZnO-170706B	Al2O3	Steel	575	30	75	20	80	No	12M	N-type	x	n
ZnO-170706C	Al2O3	Steel	575	30	75	20	80	No	500k w/o indium, 200k with indium	N-type	x	n
ZnO-170716	Al2O3	Steel	575	60	75	20	80	No	x	x	x	x
ZnO-170727A	Al2O3	Steel	575	10	75	20	80	Yes	10M	N-type	x	n
ZnO-170727B	Al2O3	Steel	575	20	75	20	80	Yes	x	N-type	x	n
ZnO-170727C	Al2O3	Steel	575	60	75	20	80	Yes	x	N-type	x	n

ZnO-170801A	Al2O3	Steel	575	10	75	20	80	Yes	x	N-type	x	n
ZnO-170801B	Al2O3	Steel	575	30	75	20	80	Yes	x	N-type	x	n
ZnO-170801C	Al2O3	Steel	575	10	75	20	80	Yes	x	N-type	x	n
ZnO-170801D	Al2O3	Steel	575	10	75	20	80	Yes	x	N-Type	x	n
ZnO-170802	Al2O3	Steel	575	10	75	20	80	Yes	x	P-type	x	p
ZnO-170815A	Al2O3	Steel	575	10	50	20	80	Yes	x	N-Type	x	n
ZnO-170815B	Al2O3	Steel	575	10	75	20	80	Yes	x	N-Type	x	n
ZnO-170815C	Al2O3	Steel	575	10	100	20	80	Yes	x	N-Type	x	n
ZnO-170823A	Al2O3	Steel	575	10	75	20	80	Yes	x	N-Type	x	n
ZnO-170823B	Al2O3	Steel	575	10	125	20	80	Yes	x	x	x	x
ZnO-170830A	Al2O3	Steel	575	60	275	20	80	Yes	x	N-Type	x	n
ZnO-170830B	Al2O3	Steel	575	60	150	20	80	Yes	x	x	x	x
ZnO-170830C	Al2O3	Steel	575	60	175	20	80	Yes	x	N-Type	x	n
ZnO-170907A	Al2O3	Steel	575	60	125	20	80	No	6.5M	Seems n-type (data from 9-19-17)	x	n
ZnO-170907B	Al2O3	Steel	575	60	125	20	80	Yes	x	x	Returned weak n-type conductivity (~10^13)	n
ZnO-170907C	Al2O3	Steel	575	60	125	20	80	No	x	x	Returned weak n-type conductivity (~10^13)	n
ZnO-170921A	Al2O3	Steel	575	60	125	20	80	No	inf	x	x	x
ZnO-170921B	glass	Steel	575	60	125	20	80	No	inf	x	x	x
ZnO-171116A	sapphire	Steel	650	30	50	20	80	Yes	10k	Yellow corner: n-type. Blue corner: p-type.	Blue chunk: n-type (-1.2E19)	n
ZnO-171116B	sapphire	Steel	650	30	50	20	80	No	inf	x	x	x
ZnO-171213	sapphire	Steel	650	2.5	75	20	80	No	inf	x	x	x
ZnO-180214A	sapphire	Steel	650	30	75	20	80	No	10k	n	x	n
ZnO-180214B	sapphire	Steel	650	30	75	20	80	No	inf	x	x	x
ZnO-180214C	sapphire	Steel	500	30	75	20	80	No	2.5M	n	x	n
ZnO-180214C (annealed)	sapphire	Steel	500	30	75	20	80	Yes	250k	n	x	n
ZnO-180217A	Sapphire	Steel	300	30	75	20	80	No	inf	x	x	x
ZnO-180217B	Sapphire	Steel	650	10	75	20	80	No	60k	n (-15mV)	n	n
ZnO-180217C	Sapphire	Steel	650	60	75	20	80	Yes	400	p (20mV)	p	p
ZnO-180228	Sapphire	Steel	650	10	75	20	80	No	1M	n (-10mV)	x	n
ZnO-180321	sapphire	Steel	650	30	75	20	80	No	55k	n (-15mV)	x	n

ZnO-180405	Sapphire	Steel	650	30	75	20	80	No	x	x	x	x
ZnO-180322	Sapphire	Steel	650	60	75	20	80	No	15K	n (-15mV)	x	n
ZnO-180502A	Sapphire	Steel	650	30	75	10	80	No	x	n (-12mV)	x	n
ZnO-180502B	Sapphire	Steel	650	30	75	5	80	No	x	n (-13mV)	x	n
ZnO-180514A	SiO2	Steel	475?	30?	75?	10	90	Yes	150K	p (20mV on average). Remeasured 1/11/19, p type (40mV)	Initially inconclusive, shown p-type on Jan 11, 2019	p
ZnO-180502B	Sapphire	Steel	650	60	75	10	90	Yes	500	p (25mV consistently). Remeasured 1/11/19, similar results	p, 10^20 carrier concentration, even several months after initial growth	p
ZnO-180612A	Sapphire	Steel	650	30	75	10	90	No				
ZnO-180612B	Sapphire	Al	650	30	75	10	90	No	500K	n (~5 mV on average)	inconclusive. Carrier concentration comes back around 10^14, and varies between p and n	n
ZnO-181105	SiN	Al	650	60	75	10	80	No	20K	p (~10 mV)	p, 10^16 carrier concentration, done without indium	p
ZnO-190131	Sapphire	Al	640	30	100	10	80	No	5K	p (~5 mV)		
ZnO-190405A	Sapphire	Al	630	30	75	10	80	No	inf	inconclusive	x	x
ZnO-190405B	Sapphire	Al	630	30	75	10	80	No	inf	inconclusive	x	x
ZnO-190405C	Sapphire	Al	630	30	75	10	80	No	10M	inconclusive	x	x
ZnO-190405D	Sapphire	Al	630	30	75	10	80	No	17M	inconclusive	x	x
ZnO-190405E	Sapphire	Al	630	30	75	10	80	No	inf	inconclusive	x	x
ZnO-190408	Sapphire	Al	650	60	75	10	80	No	30K	p (~10mV)	x	p

References

[1] Look, D. C., et al. "Electrical Properties of Bulk ZnO." *Solid State Communications*, vol. 105, no. 6, 1998, pp. 399-401. *CrossRef*, https://www.sciencedirect.com/science/article/pii/S0038109897101454, doi:10.1016/S0038-1098(97)10145-4.

[2] "kT (energy)". https://en.wikipedia.org/wiki/KT_(energy)

[3] Muth, J. F., et al. "Absorption Coefficient, Energy Gap, Exciton Binding Energy, and Recombination Lifetime of GaN obtained from Transmission Measurements." *Applied Physics Letters*, vol. 71, no. 18, 1997, pp. 2572-2574. *CrossRef*, doi:10.1063/1.120191.

[4] Look, D. C. "Recent Advances in ZnO Materials and Devices." *Materials Science & Engineering B*, vol. 80, no. 1, 2001, pp. 383-387. *CrossRef*, https://www.sciencedirect.com/science/article/pii/S0921510700006048, doi:10.1016/S0921-5107(00)00604-8.

[5] Look, D. C., Hemsky, J. W., and Sizelove, J. R.. "Residual Native Shallow Donor in ZnO." *Physical Review Letters*, vol. 82, no. 12, 1999, pp. 2552-2555. *CrossRef*, doi:10.1103/PhysRevLett.82.2552.

[6] Janotti, Anderson, and Van de Walle, Chris G. "Fundamentals of Zinc Oxide as a Semiconductor." *Reports on Progress in Physics*, vol. 72, no. 12, 2009a, pp. 126501. *CrossRef*, http://iopscience.iop.org/0034-4885/72/12/126501, doi:10.1088/0034-4885/72/12/126501.

[7] Lojek, B. *History of Semiconductors Diffusion Engineering*, September 25-27, 2002.

[8] Renlund, Gary. *personal communication*. 2016

[9] Burgener, R., et al. "As-Doped P -Type ZnO Produced by an Evaporation/sputtering Process." *Applied Physics Letters*, vol. 85, no. 22, 2004, pp. 5269-5271. *CrossRef*, http://dx.doi.org/10.1063/1.1825615, doi:10.1063/1.1825615.

[10] "Semiconductor Doping.", https://en.wikipedia.org/wiki/Doping_(semiconductor).

[11] Stewart, James Colter. "Optical Constants of evaporated amorphous zinc arsenide (Zn_3As_2) via spectroscopic ellipsometry". *BYU Physics Department Senior Thesis*, 2019

[12] Renlund, Gary. *personal communication*. 2017

[13] Peterson, J. Ryan. "Sputtering P-Type Arsenic-Doped Zinc Oxide Thin Films". *BYU Physics Department Senior Thesis*, 2018.

[14] Seebeck, Thomas J. "Magnetische Polarisation Der Metalle Und Erze Durch Temperatur-Differenz." *Abhandlungen Der Königlichen Akademie Der Wissenschaften Zu Berlin (in German).* 1822.

[15] Van der Pauw, "A Method of Measuring Specific Resistivity, and Hall Effect Of Discs Of Arbitrary Shape". *R 334 Philips Res. Repts 13, 1-9, 1958.*

[16] Gao, Fei, et al. "Microstructure and Optical Properties of Fe-Doped ZnO Thin Films Prepared by DC Magnetron Sputtering." *Journal of Crystal Growth*, vol. 371, 2013, pp. 126-129. *CrossRef*, https://www.sciencedirect.com/science/article/pii/S0022024813001504, doi:10.1016/j.jcrysgro.2013.02.027.

[17] "Cu K-Alpha.", http://gisaxs.com/index.php/Cu_K-alpha.

[18] Langford, J.I. and Wilson, A.J.C. "Scherrer after sixty years: A survey and some new results in the determination of crystallite size," J. Appl. Cryst. 11 (1978) p102-113.

[19] Bragg, William H., and Bragg, W. Lawrence. "The Reflection of X-Rays by Crystals.", no. *Proceedings of the Royal Society of London*. Series A, Containing Papers of a Mathematical and Physical Character, http://doi.org/10.1098/rspa.1913.0040.

[20] Steigmann, G.A. and Goodyear, J.. "The Crystal Structure of Cd3As2." *Acta Cryst*, vol. B24, no. 1928, 1967, pp. 1062-1067, http://journals.iucr.org/b/issues/1968/08/00/a06211/a06211.pdf.

[21] Campbell, Branton. *personal communication*. March 26, 2019

[22] Cole, H., Chambers, F. W., and Dunn, H. M.. "Lattice Parameters of Zn3As2." *Acta Crystallographica*, vol. 9, no. 8, 1956, pp. 685. *CrossRef*, https://onlinelibrary.wiley.com/doi/abs/10.1107/S0365110X5600187X, doi:10.1107/S0365110X5600187X.

Index